IEEE Open Journal of the
Industrial Electronics Society

Received 30 July 2021; accepted 28 August 2021. Date of publication 3 September 2021;
date of current version 17 September 2021. The review of this paper was arranged by Associate Editor Doriana Marilena D'Addona.

Digital Object Identifier 10.1109/OJIES.2021.3109906

Low-Cost Embedded Real-Time Handheld Vibration Smart Sensor for Industrial Equipment Onsite Defect Detection

CHAO-CHUNG PENG

Department of Aeronautics and Astronautics, National Cheng Kung University, Tainan 701, Taiwan

CORRESPONDING AUTHOR: CHAO-CHUNG PENG (e-mai: ccpeng@mail.ncku.edu.tw).

This work was supported by the Ministry of Science and Technology under Grants MOST 108-2923-E-006-005-MY3 and MOST 110-2221-E-006-095.

ABSTRACT In recent years, many industrial facilities have been required to install sensing system to monitor the health status of the equipment. Although the PC-based diagnosis system is a good alternative, it undoubtedly increases the hardware cost greatly, and also causes restrictions on system assembly. In some critical environments, installation of the PC-based system is not suitable because of high temperature, dust, and humidity. On the contrary, a high mobility portable smart sensor will be relatively adequate for onsite inspections. To solve this problem, we developed a low-cost embedded handheld smart sensor. Instead of using sophisticated algorithms, certain frequently used statistic indicators are considered. Nevertheless, due to the resource limitations of the embedded systems, it causes difficulty for real-time realization and therefore, the recursive architecture of the statistic indicators is derived. These statistical factors are then fed into a Gaussian classifier for online defect detection, which gives a great contribution to field operators for onsite inspections. The highly integrated hardware/software co-design of the developed device provides user-friendly and high mobility for field inspections. Finally, a practical industrial application regarding the online diagnosis of a solenoid valve actuator defect is presented to demonstrate the effectiveness of the developed embedded smart sensor.

INDEX TERMS Accelerometer, embedded system, industry smart sensor, online defect detection, recursive algorithm, vibration.

I. INTRODUCTION

Embedded systems have been widely integrated in smart intelligent sensing system applications [1] owing to its high security [2], compact size [3], efficient power consumption [4], high stability and affordable cost. Moreover, owing to the increment of the float point operation capability, embedded systems can even be used to realize complex algorithms [5], flight controls, sensor fusions, as well as online diagnosis [3], [6].

Among many sensors, accelerometer is one of the very common sensors used to diagnose the system status. Most of the vibration-based fault detection methods use the accelerometers as their main sensing sources. Owing to its cost and size advantages, in many semiconductor industries, the micro-electro-mechanical-systems (MEMS) type accelerometer [7] is already taken as the chief sensor for machine actuator defect online detection. To achieve immediate system monitoring and control process decision making, vibration data analysis is supposed to be made as simple and efficient as possible.

For vibration analysis [8], defect diagnosis [9], and oscillation signal analysis [10] and control [11], [12], the well-known frequency domain Fast Fourier Transform (FFT) is usually applied [13]. However, both the hardware performance, computational cost, and the demand for memory size for storing vibration data is relatively high. These issues inspire us to develop an even more cost-efficient vibration analyzer to detect anomaly of certain actuators.

To replace the FFT employed by other vibration indicators, some statistic vibration indicators are used frequently

[14]. However, calculations of these performance indicators within an interrupt routine could lead to interrupt dead-lock or interrupt stack overflow. To solve this problem, we present an efficient recursive computational architecture to compute these vibration indicators including arithmetic mean, root-mean-square (RMS), crest factor (CF), variance (VAR), standard deviation (STD), skewness (SK), and kurtosis (KT). It will be shown that the recursive computation architecture can be digested within a period of a single interrupt routine.

Contrary to the investigation targets of the works [15], [16], the handheld vibration analyzer brought forth in this paper focuses on the algorithm computational efficiency improvement. Detailed derivations are also addressed. Moreover, even though there already exist many different types of commercial handheld vibration analyzers in the market, the prices are usually not cheap and thereby they increase the development and integration costs especially for mass production. To solve these practical issues, this work presents the realization of the low-cost handheld vibration analyzer, which can be integrated into existing industrial machines for defect detection.

For reproduction purposes, the proposed recursive algorithm of these vibration indicators are first realized in an easily accessible Arduino Due board, where the computation core is a 32-bit ARM cortex-M3 84 MHz microcontroller. Since vibration is the most widely used signal to detect the mechanical faults, the work [17] investigated the fault frequency components or vibration spectrum for fault diagnosis. Therefore, FFT is also integrated into the 1st generation of our vibration analyzer prototype. However, from the perspective of end-users after a period of trial, it is even more preferable if the analyzer is able to provide whether the system is anomalous or not by using a simple defect flag "1" or "0" instead of requiring field users to read the FFT spectrum will be the best solution.

To meet this practical demand, the 2nd prototype is further refined by a size-smart and cost efficient embedded system to realize the handheld vibration analyzer, where the computation core is a 32-bit ARM cortex-M0 72 MHz microcontroller. Moreover, for defect detection decision making purposes, a Gaussian classifier is further developed. Finally, experiments are conducted to verify the application for a solenoid valve driven actuator fault online diagnosis. Note that the developed handheld module can also be extended for the online diagnosis of actuator driven mechanical systems in other industrial fields.

The main contribution of this paper include: derivations of the statistic measurement indices in the recursive forms; computational efficient embedded architecture for algorithm realization; applying Gaussian classifier for detect detection; hardware/software co-design of a low-cost handheld smart vibration analyzer, and finally, a practical case study is presented to validate the feasibility of the developed smart sensor. Put it simply, the developed smart handheld vibration analyzer can be used to detect whether an actuator, e.g., a solenoid valve, is going to be defective.

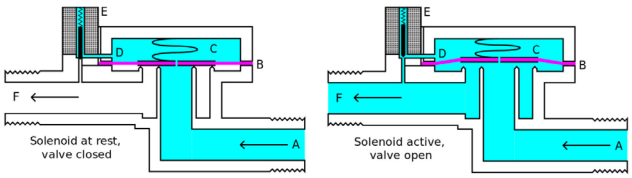

FIGURE 1. Operation concept demonstration of the solenoid valve (adapted from Wikipedia).

II. PROBLEM STATEMENT

High speed solenoid valves have been widely utilized in manufacturing processes and semiconductor machines due to its performance on the flow rate modulation. However, after a period of operations, certain defects will be induced on the machines due to the high speed reciprocating operations. These defects, which are invisible, result in the degradation of the product line mass product quality; therefore it should be prevented in advanced. From the viewpoint of real applications, this studies focuses on the development of a smart embedded real-time vibration analyzer for detecting the potential defect of a high speed on/off type solenoid valve [18], which is widely used in a semiconductor manufacturing processes. A solenoid valve, as illustrated in Fig. 1, is an electromechanically operated valve, which can be used to regulate a flow rate.

In many industrial manufacturing processes, the solenoid valves are operated at a high on-off frequency in order to ensure high product throughput. However, it has been found that after a period of operations, certain tears and wears are inevitably induced. Such the defects cannot be detected via direct visual inspection. In order to address this issue, the status of the solenoid valve needs to be monitored regularly. For the sake of this demand, the developed vibration analyzer will be integrated into the equipment.

The first generation of the vibration analyzer, which is illustrated in Fig. 2(a), is developed. The hardware configuration of Fig. 2(a) mainly includes a vibration sensor, a TFT touch screen, and a development board. The sensor considered in this prototype is the analog output MEMS type ADXL-337 accelerometer, which is the same one applied in [3]. For the development cost attenuation and easy reproduction for readers, the well commercialized ARM cortex-M3 Arduino due board is implemented. The total cost is less than 60 USD.

For vibration analysis, the microcontroller is applied to realize the real-time FFT, where the sampling rate is 4 KHz. Fig. 2(b) illustrates the FFT spectrum of a normal solenoid valve. The main vibration peaks appear around 250 Hz, 500 Hz, 750 Hz and so on. In regard to the defected one, as shown in Fig. 2(c), we can find that once the defect inside the solenoid valve occurs, there came out a couple of extra frequency clusters located at around 105 Hz, 125 Hz and 144 Hz appeared in the FFT spectrum. These clusters give us a great insight for solenoid defect detection and for further maintenance decision making.

Unfortunately, in practices, reading and understanding the FFT spectrum challenge local inspectors. According to the

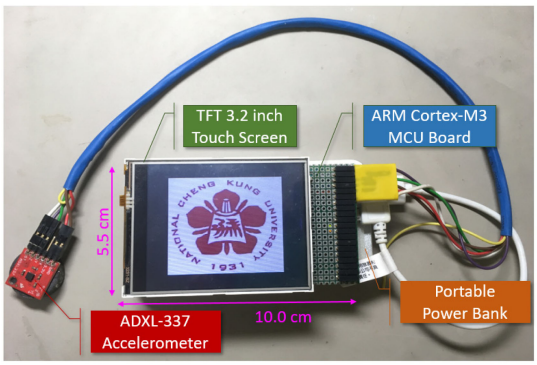

(a). Prototype of the handheld vibration analyzer.

(b). Normal solenoid valve FFT spectrum.

(c). Abnormal solenoid valve FFT spectrum.

FIGURE 2. On-site experiment of a mechanical system for the solenoid valve defect detection, (a) prototype of the handheld vibration analyzer, (b) the normal FFT spectrum, and (c) the abnormal FFT spectrum.

preliminary result, it inspires us to further development an even more cost-efficient and easy-to-read embedded device that is able to deliver the message regarding the health status of the solenoid valve without the use of the informative FFT. As a result, in this study, some useful measurements such as the time domain vibration indicators are used to point out whether the operating solenoid valve needs to be replaced.

Furthermore, according our past experiences returned by field workers, the TFT touch screen usually causes an anomaly after a period of usage. Second, it is electricity burden such that a power bank is needed to support it endurance. Third, the total weight is higher than 300 grams, which is even heavier than a user-friendly smartphone. To remove these drawbacks, a 2nd generation handheld vibration smart sensor is going to be presented.

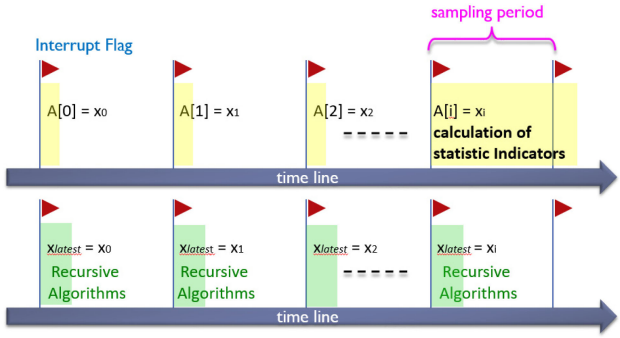

FIGURE 3. Real-time architecture in the embedded system.

The removal of the TFT touch can bring the following advantages: 1). reducing the chance of malfunction occurrence, 2). reducing the total weight including power bank removal, 3). reducing the total size, 4). Reducing the total price. The cost saving is mainly contributed by discarding the use of a TFT touch screen and a power bank. Based on these advantages, the 2nd generation smart sensor is able to provide much better user-friendly usage experience. Since the 2nd generation of the handheld vibration analyzer is without the TFT touch screen, we integrated a Bluetooth device in it. As a result, the analyzer can send the diagnosis information to our smartphone via Bluetooth connection.

III. REAL-TIME RECURSIVE STATISTIC INDICATORS

Practically speaking, undesirable vibrations can lead to accelerated aging and fatigue, which could be detrimental to the machine's life cycle. Defected solenoid valves could lead to unstable flow control and thereby degrade the final product quality. Therefore, monitoring and detecting such abnormal vibrations would be indispensable. For this purpose, the well-known FFT is usually applied first for prior analysis. Nevertheless, FFT spectrum cause dramatic difficulty for onsite inspectors to understand. To address this practical issue, we tend to use other measurement indices, such as mean, RMS, CF, VAR, STD, SK, and KT, are used to evaluate the level of the vibrations.

Since the memory of a MCU is quite limited. Generation of large size arrays causes memory burden. More importantly, for the collected data arrays, the associated computations of the measurement indices give rise to inefficient performance.

For the proposed real-time architecture, it consists of a polling loop and a timer interrupt loop. The polling loop is used to deal with the calculation of FFT while the interrupt loop is used to receive the latest vibration data and calculate the vibration indicators. Since there is only one core in the MCU, it becomes a multi-task programming problem. Fig. 3 illustrates the main issue of the algorithm realization of the indicators in an embedded system. As shown at the upper part of Fig. 3, at every interrupt routine, if the MCU only considers the latest data collection, then at a certain interrupt, computational time consumption of the statistic vibration indicators

is going to be longer than a single sampling period. Put it simply, the value of these statistic vibration indicators cannot be refreshed within a single interrupt in-time. It could give rise to unexpected interrupt dead-lock or interrupt stack overflow.

On the contrary, as shown at the lower part of Fig. 3, if the value of the indicators can be updated at each interruption, there is no need to create an extra array and the unstable interrupt routine problem can be solved as well.

Therefore, in the following, computations of these statistic vibration indicators are reconsidered and the corresponding computations are going to be reformulated in terms of recursive forms, which are very suitable for the realizations at each interrupt subroutine in an embedded system.

A. RECURSIVE MEAN, RMS AND CF

For each timer interrupt, the latest accelerometer output data is going to be measured by the MCU. Define the accelerometer data as x_i, then for a period of time, the mean value can be computed by

$$\mu = \frac{1}{n}\sum_{i=1}^{n} x_i \tag{1}$$

where n represents the total size of the measurements. Apparently, a large storage size is required to locate the historical data. Moreover, the computation involves $n-1$ additions, which may not be realizable in-time within a single interrupt cycle.

It is well known that (1) can be easily expressed as the following recursive form

$$\mu_n = \frac{n-1}{n}\mu_{n-1} + \frac{1}{n}x_n \tag{2}$$

Based on the recursive property, computation of (2) can be easily digested within an interrupt cycle since it only requires very few arithmetic operations.

For the RMS, the definition is

$$x_n^{rms} = \sqrt{\frac{1}{n}\sum\nolimits_{i=1}^{n} x_i^2} = \sqrt{\frac{1}{n}\left(x_1^2 + x_2^2 + \cdots + x_n^2\right)} \tag{3}$$

Similar to the procedure as the one presented in (2), define a new variable as

$$\begin{aligned} x_n^{ss} &= \frac{1}{n}\sum_{i=1}^{n} x_i^2 \\ &= \frac{n-1}{n}\cdot\frac{1}{n-1}\left(x_1^2 + x_2^2 + \cdots + x_{n-1}^2\right) + \frac{1}{n}x_n^2 \\ &= \frac{n-1}{n}\cdot x_{n-1}^{ss} + \frac{1}{n}x_n^2 \end{aligned} \tag{4}$$

Based on (4), the recursive form of (3) can be expressed as

$$x_n^{rms} = \sqrt{x_n^{ss}} \tag{5}$$

For the CF, recall the definition, the formula is

$$C_F = x_{\max}^{abs}/x_n^{rms} \tag{6}$$

where $x_{\max}^{abs}$ represents the maximum absolute value. Therefore, for each timer interrupt, the calculation of recursive C_F needs to detect the latest maximum value and to replace the old one when a new maximum absolute data appears. That is, the one-in-one-out criterion is used

$$x_{\max}^{abs} \leftarrow \max\left(x_{\max}^{abs}, |x_i|\right) \tag{7}$$

With the aid of (4), (5) and (7), it can be seen that the CF defined in (6) can be refreshed immediately at each interruption.

B. RECURSIVE VARIANCE AND STANDARD DEVIATION

Variance is also a widely used measurement index for vibration analysis. The variation of vibrations responds to the characteristics of mechanical structures and indicates how far the systems deviate from the normal status.

By definition, the variance is

$$v_n(x) = \frac{1}{n}\sum_{i=1}^{n}(x_i - \mu)^2 \tag{8}$$

Once a bunch of data is gathered and stored in a large size array, calculation of (8) proposes no difficulty. Nevertheless, it will result in computation burden in view of a timer interrupt. To address this issue, the recursive form is also studied. To obtain the recursive formula, we consider an auxiliary variable as follows

$$S = \sum_{i=1}^{n}(x_i - \mu)^2 \tag{9}$$

It is obvious that once (9) can be calculated iteratively, the formulas for the recursive variance (8), as well as the recursive standard deviation can be achieved simultaneously.

For the n^{th} timer interrupt, (9) can be re-represented by

$$\begin{aligned} S_n &= (x_n - \mu_n)^2 + \sum_{i=1}^{n-1}(x_i - \mu_{n-1} + \mu_{n-1} - \mu_n)^2 \\ &= (x_n - \mu_n)^2 + \sum_{i=1}^{n-1}(x_i - \mu_{n-1})^2 \\ &\quad + 2(\mu_{n-1} - \mu_n)\sum_{i=1}^{n-1}(x_i - \mu_{n-1}) \\ &\quad + (n-1)(\mu_{n-1} - \mu_n)^2 \end{aligned} \tag{10}$$

Also note that

$$\begin{cases} S_{n-1} = \sum_{i=1}^{n-1}(x_i - \mu_{n-1})^2 \\ 2(\mu_{n-1} - \mu_n)\sum_{i=1}^{n-1}(x_i - \mu_{n-1}) = 0 \end{cases} \tag{11}$$

Eq. (10) and (11) yield the following recursive update law

$$S_n = S_{n-1} + (x_n - \mu_n)^2 + (n-1)(\mu_{n-1} - \mu_n)^2 \tag{12}$$

Hence, the recursive variance can be finally represented as

$$\begin{aligned} v_n(x) &= \frac{1}{n}\cdot S_n \\ &= \frac{n-1}{n}\cdot\frac{S_{n-1}}{n-1}+\frac{(x_n-\mu_n)^2}{n}+\frac{n-1}{n}(\mu_{n-1}-\mu_n)^2 \\ &= \frac{n-1}{n}v_{n-1}(x)+\frac{(x_n-\mu_n)^2}{n}+\frac{n-1}{n}(\mu_{n-1}-\mu_n)^2 \end{aligned} \tag{13}$$

where the recursive mean μ_n is already available from the recursive mean as illustrated in (2).

Eq. (13) gives the recursive standard deviation without the need of further derivation; that is

$$\sigma_n = \sqrt{v_n(x)} \tag{14}$$

C. RECURSIVE SKEWNESS AND KURTOSIS

Skewness and kurtosis are both useful indicators that quantifies whether the histogram of the data distribution matches the Gaussian distribution [19]. However, the recursive forms of the skewness, as well as kurtosis, are often less studied.

In the following derivations, we are going to illustrate that there exists strong connections between the recursive mean, recursive variance, recursive standard deviation, and the recursive skewness/kurtosis.

Recall the definition of skewness [19]

$$S^K = \frac{E(x-\mu)^3}{\sigma^3} = \frac{\frac{1}{n}\sum_{i=1}^{n}(x_i-\mu)^3}{\sigma^3} \tag{15}$$

Based on the similar concept of the previous subsection, define an auxiliary variable as follows

$$S_n^s = \frac{1}{n}\sum_{i=1}^{n}(x_i-\mu_n)^3 \tag{16}$$

It is clear that the recursive skewness is available as long as the sum of the cubic terms S_n^s is obtained.

$$\begin{aligned} S_n^s &= \frac{1}{n}(x_n-\mu_n)^3+\frac{1}{n}\sum_{i=1}^{n-1}(\underbrace{x_i-\mu_{n-1}}_{A}+\underbrace{\mu_{n-1}-\mu_n}_{B})^3 \\ &= \frac{1}{n}(x_n-\mu_n)^3+\frac{n-1}{n}\cdot\frac{1}{n-1}\sum_{i=1}^{n-1}A^3 \\ &\quad+\frac{3B}{n}\sum_{i=1}^{n-1}A^2+3B^2\frac{1}{n}\sum_{i=1}^{n-1}A+\frac{(n-1)}{n}B^3 \end{aligned} \tag{17}$$

Note that

$$\begin{aligned} S_{n-1}^s &= \frac{1}{n-1}\sum_{i=1}^{n-1}A^3, \quad \sum_{i=1}^{n-1}A = 0 \\ \mathrm{var}_{n-1}(x) &= \frac{1}{n-1}\sum_{i=1}^{n-1}(x_i-\mu_{n-1})^2 \end{aligned} \tag{18}$$

Substituting (18) into (17) gives

$$\begin{aligned} S_n^s &= \frac{n-1}{n}\cdot S_{n-1}^s+\frac{1}{n}(x_n-\mu_n)^3 \\ &\quad+\frac{3(\mu_{n-1}-\mu_n)(n-1)}{n}\cdot v_{n-1}(x) \\ &\quad+\frac{(n-1)}{n}(\mu_{n-1}-\mu_n)^3 \end{aligned} \tag{19}$$

As a result, the recursive skewness can be expressed as

$$S_n^K = S_n^s/\sigma_n^3 \tag{20}$$

where σ_n is acquired from the recursive variance derived in (13) and (14).

For the kurtosis, its definition [20] is

$$K^O = \frac{E(x-\mu)^4}{\sigma^4} = \frac{\frac{1}{n}\sum_{i=1}^{n}(x_i-\mu)^4}{\sigma^4} \tag{21}$$

Similarly, the recursive kurtosis is available as long as the term

$$S^o = \frac{1}{n}\sum_{i=1}^{n}(x_i-\mu)^4 \tag{22}$$

can be reformulated as a recursive form.

Examining (22), it is equivalent to

$$\begin{aligned} S_n^o &= \frac{1}{n}(x_n-\mu_n)^4+\frac{1}{n}\sum_{i=1}^{n-1}(\underbrace{x_i-\mu_{n-1}}_{A}+\underbrace{\mu_{n-1}-\mu_n}_{B})^4 \\ &= \frac{1}{n}(x_n-\mu_n)^4+\frac{1}{n}\sum_{i=1}^{n-1}\begin{pmatrix}A^4+4A^3B+6A^2B^2\\+4AB^3+B^4\end{pmatrix} \end{aligned} \tag{23}$$

Based on the previous derived formulas, it can be found that

$$\begin{aligned} S_{n-1}^o &= \frac{1}{n-1}\sum_{i=1}^{n-1}A^4, \quad \sum_{i=1}^{n-1}AB^3 = 0 \\ S_{n-1} &= \frac{1}{n-1}\sum_{i=1}^{n-1}(x_i-\mu_{n-1})^3 \\ v(x)_{n-1} &= \frac{1}{n-1}\sum_{i=1}^{n-1}(x_i-\mu_{n-1})^2 \end{aligned} \tag{24}$$

Based on (24), (23) is further simplified to

$$\begin{aligned} S_n^o &= \frac{n-1}{n}S_{n-1}^o+\frac{1}{n}(x_n-\mu_n)^4 \\ &\quad+\frac{4(\mu_{n-1}-\mu_n)(n-1)}{n}\cdot S_{n-1}^s \\ &\quad+\frac{6(\mu_{n-1}-\mu_n)^2(n-1)}{n}\cdot v(x)_{n-1} \\ &\quad+\frac{n-1}{n}(\mu_{n-1}-\mu_n)^4 \end{aligned} \tag{25}$$

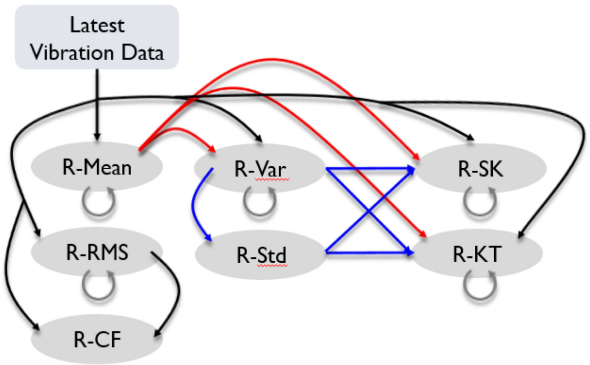

FIGURE 4. Pipeline of the recursive algorithm during each interrupt.

Therefore, the value of the kurtosis at the n^{th} MCU interrupt can be updated immediately by calculating

$$K_n^O = S_n^o/\sigma_n^4 \tag{26}$$

The pipeline of the proposed recursive algorithm overview is illustrated in Fig. 4, where the R-Mean, R-RMS, R-CF, R-Var, R-Std, R-SK, and R-KT represent recursive mean, recursive RMS, recursive CF, recursive variance, recursive standard deviation, recursive skewness and recursive kurtosis, respectively. Fig. 4 clearly shows that the R-SK and R-KT can be easily obtained providing the R-Mean, R-Var, and R-Std which are readily available.

In conclusion, once the latest vibration data is collected by the MCU through an analog-to-digital converter (ADC) interface at each timer interrupt, the related recursive algorithms are executed and the values of the vibration indicators can be immediately refreshed within a single cyclic interrupt.

Remark: Providing the conventional computation method is applied, the seven indicators are calculated one-by-one. It is time exhausted for a MCU to digest so many arithmetic operations (ex. addition, subtraction, multiplication, division, power, and so on) within a millisecond. On the contrary, by using the proposed recursive method, it will be shown later that the maximum time cost to update the indicators is only 145 microseconds. The significant contributions come from the derived recursive formula of the indicators and the pipeline presented in Fig. 4. It shows that not only the recursive forms are used, many calculations can be re-used as well. This configuration saves quite a lot time for real-time computation and avoids memory burden in the resource limited low cost MCU.

IV. DEFECT GAUSSIAN MODEL CONSTRUCTION

Based on the recursive algorithms, a collection of statistical data is available for defect model construction. For defect model construction purposes, the measurements are collected from a normal solenoid valve vibration data and from an abnormal one, respectively. A Gaussian classifier is considered, where the probability density function (PDF) of a Gaussian is

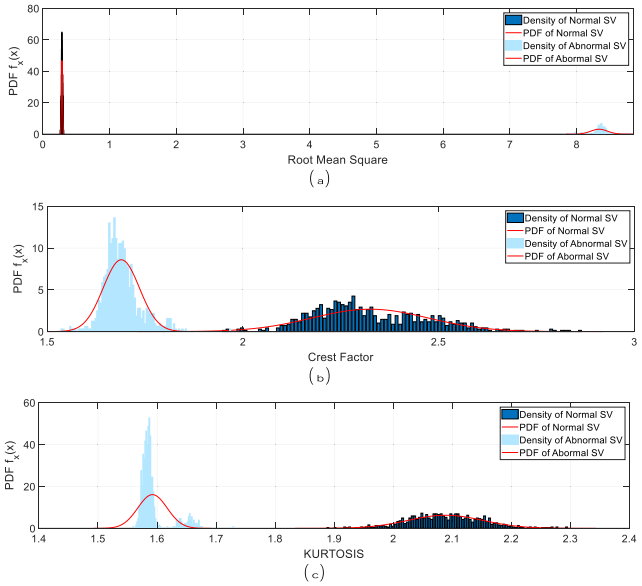

FIGURE 5. Illustrated PDFs of the vibration indicators: (a) RMS, (b) CF and (c) KT.

described by

$$P\left(x|\mu_G, \sigma_G^2\right) = \frac{1}{\sigma_G\sqrt{2\pi}} \exp\left(-\frac{(x-\mu_G)^2}{2\sigma_G^2}\right) \tag{27}$$

where μ_G and σ_G represent the set of the mean and standard deviation of the vibrator indicators, respectively, which are defined by

$$\begin{aligned} \mu_G &:= \left\{ \mu_G \in \mathbb{R}^\ell \;\middle|\; \begin{array}{l} \mu_{MEAN},\ \mu_{RMS},\ \mu_{CF}, \\ \mu_{STD},\ \mu_{\text{VAR}},\ \mu_{SK},\ \mu_{KT} \end{array} \right\} \\ \sigma_G &:= \left\{ \sigma_G \in \mathbb{R}^\ell \;\middle|\; \begin{array}{l} \sigma_{MEAN},\ \sigma_{RMS},\ \sigma_{CF}, \\ \sigma_{STD},\ \sigma_{\text{VAR}},\ \sigma_{SK},\ \sigma_{KT} \end{array} \right\} \end{aligned}, \ell = 7 \tag{28}$$

The associated PDFs, for example, RMS, CF, and KT, from the seven indicators are illustrated in Fig. 5. For defect detection purposes, the selected indicators should be distinguishable between the normal condition and abnormal condition in terms of the PDF. Apparently, these vibration indicators can be used as the candidates for constructing the Gaussian classifier. Since the associated Gaussian model for each indicator is obtained, it can be represented as a multivariate Gaussian model as shown in Fig. 6.

V. DEFECT CLASSIFICATION PROBABILITY MODEL

During the online inspection, the handheld embedded vibration analyzer should be able to provide information on whether the actuator is healthy or not. Then the replacement decision or a warning flag will be made accordingly. Although in recent years, many different machine learning skills were developed such as support vector machine [21], convolution neural network [22], these methodologies usually count on high performance computation units and thereby inevitably raising the software/hardware cost. Moreover, the training procedures of the aforementioned methods are hard

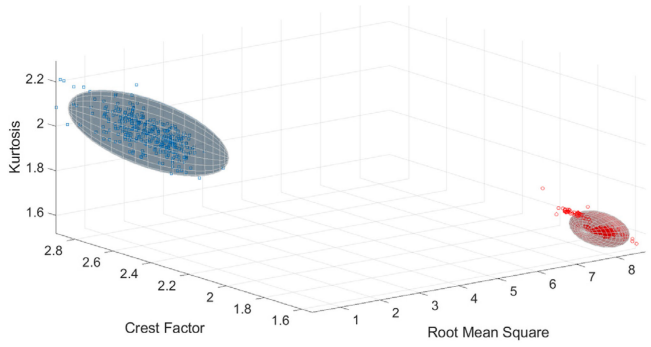

FIGURE 6. Constructed multivariate Gaussian model for the 3D case visualization.

to be realized in a low-cost embedded system. For engineering practices, the main priority of this paper is to develop a cheap, portable and with decision-making embedded device using a low-cost and resource limited MCU. Therefore, the classifier should be made as simple as possible. Based on these practical demands, the idea of the Gaussian Naive Bayes (GNB) classifier [23] is adopted.

The GNB classifier is based on a conditional probabilistic model, where the probability can be represented by

$$P\left(C_k|x_1, x_2, \cdots, x_n\right) := P\left(C_k|\mathbf{x}\right) = \frac{P\left(C_k \cap \mathbf{x}\right)}{P\left(\mathbf{x}\right)} \tag{29}$$

The Bayes' rule shows that

$$P\left(C_k|\mathbf{x}\right) P\left(\mathbf{x}\right) = P\left(\mathbf{x}|C_k\right) P\left(C_k\right) \tag{30}$$

Eq. (29) implies that given a sample, represented by a vector $\mathbf{x}$ including n features, to be classified, calculate $P(C_k|\mathbf{x})$ for each k possible classes denoted by C_k.

Applying the chain rule for (29) gives

$$\begin{aligned} P\left(C_k \cap \mathbf{x}\right) &= P\left(\mathbf{x} \cap C_k\right) \\ &= P\left(x_1, x_2, \cdots, x_n, C_k\right) \\ &= P\left(x_1|x_2, \cdots, x_n, C_k\right) P\left(x_2, \cdots, x_n, C_k\right) \\ &\quad \vdots \\ &= P\left(x_1|x_2, \cdots, x_n, C_k\right) P\left(x_2|x_3, \cdots, x_n, C_k\right) \\ &\quad \times \cdots \times P\left(x_{n-1}|x_n, C_k\right) P\left(x_n|C_k\right) P\left(C_k\right) \end{aligned} \tag{31}$$

Consider that all the features in feature space $\mathbf{x}$ are mutually independent, (31) can be simplified to

$$P\left(C_k \cap \mathbf{x}\right) = P\left(C_k\right) \cdot \prod_{i=1}^{n} P\left(x_i|C_k\right) \tag{32}$$

Recall the conditional probability, it gives

$$P\left(\mathbf{x}|C_k\right) = \frac{P\left(\mathbf{x} \cap C_k\right)}{P\left(C_k\right)} = \frac{P\left(C_k \cap \mathbf{x}\right)}{P\left(C_k\right)} \tag{33}$$

From (32), (33) can be simplified to

$$\begin{aligned} P\left(\mathbf{x}|C_k\right) &= \frac{P\left(C_k\right) \cdot \prod_{i=1}^{n} P\left(x_i|C_k\right)}{P\left(C_k\right)} \\ &= \prod_{i=1}^{n} P\left(x_i|C_k\right) \end{aligned} \tag{34}$$

From (29) and (32), the probability of the classification given sample data can be calculated with

$$P\left(C_k|\mathbf{x}\right) = \frac{P\left(C_k\right) \cdot \prod_{i=1}^{n} P\left(x_i|C_k\right)}{P\left(\mathbf{x}\right)} \tag{35}$$

where

$$\begin{aligned} P\left(\mathbf{x}\right) &= \sum_{j=1}^{k} P\left(\mathbf{x} \cap C_j\right) \\ &= \sum_{j=1}^{k} \left(P\left(\mathbf{x}|C_j\right) P\left(C_j\right)\right) \end{aligned} \tag{36}$$

Based on (36), the probability (35) of the classification can be further represented by

$$\begin{aligned} P\left(C_k|\mathbf{x}\right) &= \frac{P\left(C_k\right) \cdot \prod_{i=1}^{n} P\left(x_i|C_k\right)}{\sum_{j=1}^{k} \left(P\left(\mathbf{x}|C_j\right) P\left(C_j\right)\right)} \\ &= \frac{P\left(C_k\right) \cdot \prod_{i=1}^{n} P\left(x_i|C_k\right)}{\sum_{j=1}^{k} \left(\prod_{i=1}^{n} P\left(x_i|C_j\right) P\left(C_j\right)\right)} \end{aligned} \tag{37}$$

In our application, there are only two outcomes and thus $k = 2$. One of which is normal class C_1 and the other an abnormal class C_2. It can be shown that $\sum_{j=1}^{k} P(C_j|\mathbf{x}) = 1$.

The details are shown as below

$$\begin{aligned} \sum_{j=1}^{k=2} P\left(C_j|\mathbf{x}\right) &= \sum_{j=1}^{k=2} \left(\frac{P\left(C_j\right) \cdot \prod_{i=1}^{n} P\left(x_i|C_j\right)}{\sum_{j=1}^{k} \left(\prod_{i=1}^{n} P\left(x_i|C_k\right) P\left(C_j\right)\right)} \right) \\ &= \frac{P\left(C_1\right) \cdot \prod_{i=1}^{n} P\left(x_i|C_1\right)}{\prod_{i=1}^{n} P\left(x_i|C_1\right) P\left(C_1\right) + \prod_{i=1}^{n} P\left(x_i|C_2\right) P\left(C_2\right)} \\ &\quad + \frac{P\left(C_2\right) \cdot \prod_{i=1}^{n} P\left(x_i|C_2\right)}{\prod_{i=1}^{n} P\left(x_i|C_1\right) P\left(C_1\right) + \prod_{i=1}^{n} P\left(x_i|C_2\right) P\left(C_2\right)} \\ &= 1 \end{aligned} \tag{38}$$

Therefore, (38) provides a useful index and can be used to evaluate the health condition of the solenoid valve. Put it simply, once the health condition of the solenoid valve goes below to 0.5, the actuator defect flag "1" will be triggered. In other words, for the proposed handheld vibration smart sensor, the end-users do not necessarily need to read the seven measurement indicators and they can make the maintenance decision making immediately according to the classifier return.

In practice, for our testing factory, there are experts who are qualified to evaluate whether the solenoid valves are normal or abnormal. Based on their specialty, these solenoids valves are separated into two groups: normal and abnormal. The abnormal solenoid valves were obtained naturally evolved over time. For the normal solenoid valve group and the abnormal

TABLE 1. Status Normality and Abnormality Evaluation Criterion

Probability Value	Normal Condition $P(C_1 \mid \mathbf{x})$	Abnormal Condition $P(C_2 \mid \mathbf{x})$
Threshold	α	$1-\alpha$

one, we apply the same standard operation procedures. Meanwhile, the associated vibration data are collected correspondingly for Gaussian classifier construction. Therefore, based on the probability criterion table as shown in Table 1, the smart sensor is able to evaluate the tested solenoid valve is normal or abnormal.

For Table 1, a typical probability setting is "$\alpha = 0.5$". It means once the probability of the normal condition is higher than the probability of the abnormal condition, the fault flag will be triggered. However, if $\alpha = 0.9$ is set, it implies that the tested solenoid valve must be very well-conditioned. Otherwise, it will be treated as abnormal. On the contrary, when $\alpha = 0.1$ is set. Even if the status of the tested solenoid valve is under degradation, it is still being treated as a normal one. Under this situation, the fault alarm will not be triggered until $\alpha < 0.1$. In conclusion, the value of α is used to adjust the conservativeness when evaluating whether the solenoid valve is normal or not. Put is simply, the larger the α, the higher the conservativeness.

VI. DIAGNOSIS PROCEDURE AND EMBEDDED SMART SENSOR PROTOTYPE DEVELOPMENT

From the viewpoint of the practical usage procedures, the users have to collect the vibration data coming from the normal solenoid valve and the abnormal one separately. When constructing the diagnosis model, the vibration signal flow is going to be fed into a 1st Order high pass filter in which the high cut-off frequency is 1 Hz. The output of the filtered vibration signals are then sent into the proposed recursive algorithms as presented in Section III. The recursive algorithms are executed on the raw data at 4 KHz interrupt and are used to refresh the latest statistical value of the indicators every 0.25 seconds. The 4 Hz update rate is applied with the consideration of end-users' comfortability. Too fast update rate shown on the smartphone screen will cause difficult and dizziness to end-users. Based on the 4 Hz indicator update rate, the recursive algorithms are once again applied for multivariate Gaussian model constructions, which are represented in (27) and (28). So far the training procedure is completed.

Next, the procedure will be switched to the testing mode. An unknown signal flow collected from another solenoid valve will be fed into the recursive algorithms and the resulting value of the indicators are further sent to the pre-trained Gaussian model. Next, the associated probability will be evaluated using (37) and the actuator replacement decision making can be made accordingly. Fig. 7 summarizes the above procedures of the developed handheld vibration analyzer. All the training and testing algorithms are realized in the embedded system in terms of recursive architecture. Therefore,

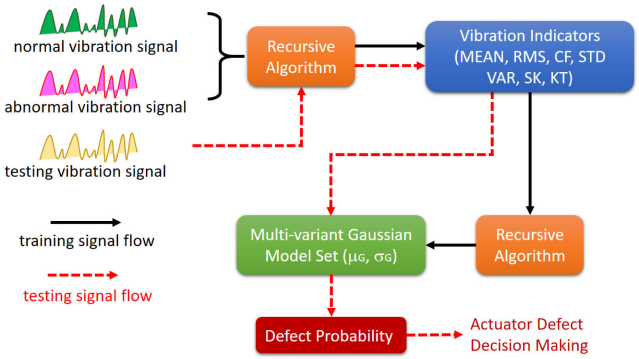

FIGURE 7. Flow chart of the defect detection algorithm in an embedded system.

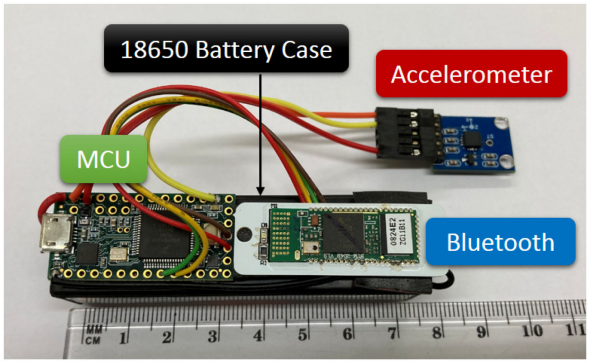

FIGURE 8. The 2nd generation of the handheld low-cost vibration analyzer.

the online inspection-and-diagnosis device can be made even cheaper, smaller, and smarter.

With the aid of the training/testing procedures designed in the proposed smart handheld vibration analyzer, the end-users do not necessarily need to read these measurement indicators and they can make the maintenance decision making immediately according to the Gaussian classifier return. This mechanism gives great contribution to fresh field operators who are not with related system diagnosis training and mathematical background.

In order to minimize the size and cost of the handheld vibration analyzer, the 2nd generation vibration analyzer was developed and is shown in Fig. 8, where the MCU is the 72MHz ARM Cortex-M4. An extra Bluetooth module is integrated for future IoT use. The total weight including a 18650 battery is about 62 grams and the total hardware cost is less than 30 USD.

To evaluate the proposed recursive algorithms as summarized in Figs. 4 and 7 running in the 2nd generation vibration analyzer, the execution procedure time cost was recorded. Apparently, Fig. 9 shows that for the 4 KHz interrupt, the recursive algorithms can be digested completely within 145 micro seconds. Therefore, to avoid interrupt stack overflow, we set 250 microseconds for the interrupt routine. Based on this interrupt setting, their remains 100 microseconds more left to

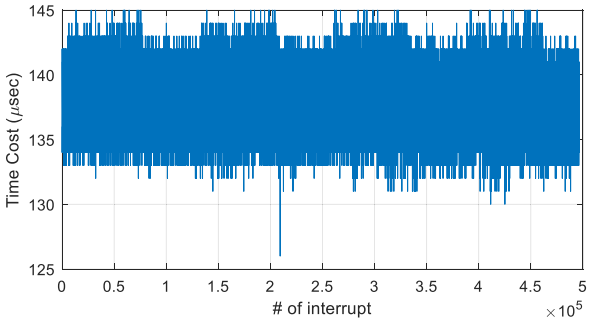

FIGURE 9. Real time performance evaluation of the recursive algorithm in an embedded system.

execute other data handshake and function creations for future development.

Finally, to validate the feasibility of the 2nd generation low-cost handheld vibration analyzer, the device is integrated into a solenoid valve based servo mechanical system for online defect detection purposes. Since the solenoid valve is working with a high frequency and fast reciprocating behavior, it causes wear and tear after a certain period of time usage. The wear of the valve is going to deteriorate the final mass product quality and therefore it should be prevented for quality control purposes.

For our specific application in solenoid valve defect detection, we collected extra 100 data sets from other normal and abnormal solenoid valves, respectively. Then, these data are being classified by the procedures as illustrated in Fig. 7. Note that the procedures are realized in the integrated embedded system as shown in Fig. 8. So far, we can achieve almost 100 percentages correct classification rate, which demonstrates the accuracy classification model. However, the perfect result may come from that the testing samples remain limited. Moreover, a corner case would be the early detection of a fault that just begins to show some premature signs of failure. For this corner case, if $\alpha = 0.5$ is applied, the sensor will return "Normal". For practical diagnosis, it is always difficult to define a clear threshold when the solenoid valve is called abnormal. The aforementioned perfect results may come from the well-developed fault states of the solenoid valves provided by local operators. Based on this situation, the fault can be distinguished easily. Even so, we can still expect that the accuracy of the proposed method can achieve up to 95%. Experiments testify the efficiency and feasibility of the proposed low-cost handheld smart sensor.

VIII. CONCLUSION

In this paper, a computation efficient real-time diagnosis computation architecture is presented and a low-cost real-time handheld vibration analyzer is developed. The developed smart device is able to achieve the actuator health status inspections. To evaluate the performance and the applicability of the low-cost handheld smart sensor, it is integrated into a solenoid valve driven servo mechanical system for online diagnosis purposes. Under the restricted demands on the development cost, size, weight and limited embedded system computation memory resources, we developed a computational efficient real-time architecture and related recursive formulas of vibrations indicators. The recursive algorithms and the classification procedures have been successfully implemented into a low-cost 2nd generation handheld vibration analyzer. The developed handheld vibration analyzer can also be extended for other mechanical systems for defect detection purposes. For the actuator defect detection application considered in this paper, the outcome shows a good defect classification performance. Experimental results demonstrate the efficiency of the recursive computation architecture and the feasibility for online defect detection. Owing to the high integrated hardware/software co-design, the proposed smart sensor is suitable for product commercialized.

ACKNOWLEDGMENT

The author would like to thank Dr. Chung-Yung Wu, now a section manager of Automation & Instrument System Development Section, Research & Development Department, China Steel Corporation, for providing a great opportunity to discuss the related functions for smart sensor designs. Special thanks are also dedicated to his helpful advices on various technical issues examined in this paper.

REFERENCES

[1] S. Ryu and S. Kim, "Embedded identification of surface based on multirate sensor fusion with deep neural network," *IEEE Embedded Syst. Lett.*, vol. 13, no. 2, pp. 49–52, Jun. 2020.

[2] J. Chen, H. Guo, and W. Hu, "Research on improving network security of embedded system," in *Proc. 6th IEEE Int. Conf. Cyber Secur. Cloud Comput./5th IEEE Int. Conf. Edge Comput. Scalable Cloud*, 2019, pp. 136–138.

[3] S. Ardalan, S. Moghadami, and S. Jaafari, "Motion noise cancelation in heartbeat sensing using accelerometer and adaptive filter," *IEEE Embedded Syst. Lett.*, vol. 7, no. 4, pp. 101–104, Dec. 2015.

[4] S. Daud, R. B. Ahmad, and N. S. Murhty, "The effects of compiler optimizations on embedded system power consumption," in *Proc. Int. Conf. Electron. Des.*, 2008, pp. 1–6.

[5] N. B. Amor, M. Baklouti, K. Barhoumi, and M. Jallouli, "Efficient embedded software implementation of a low cost robot localization system," in *Proc. IEEE Int. Conf. Des. Test Integr. Micro Nano-Syst.*, 2019, pp. 1–5.

[6] J. Kim and C. Chu, "Analysis and modeling of selected energy consumption factors for embedded ECG devices," *IEEE Sensors J.*, vol. 16, no. 6, pp. 1795–1805, Mar. 2016.

[7] S. Wang, X. Wei, Y. Zhao, Z. Jiang, and Y. Shen, "A MEMS resonant accelerometer for low-frequency vibration detection," *Sensors Actuators A: Phys.*, vol. 283, pp. 151–158, 2018.

[8] H. Sun, S. Yuan, and Y. Luo, "Cyclic spectral analysis of vibration signals for centrifugal pump fault characterization," *IEEE Sensors J.*, vol. 18, pp. 2925–2933, Apr. 2018.

[9] A. Lay-Ekuakille, G. Vendramin, and A. Trotta, "Robust spectral leak detection of complex pipelines using filter diagonalization method," *IEEE Sensors J.*, vol. 9, no. 11, pp. 1605–1614, Nov. 2009.

[10] F. Lee, G. Zhou, H. Yu, and F. S. Chau, "A MEMS-based resonant-scanning lamellar grating fourier transform micro-spectrometer with laser reference system.," *Sensors Actuators A: Phys.*, vol. 149, pp. 221–228, 2009.

[11] G. Sapra, M. Sharma, R. Vig, and S. Sharma, "Multiwalled carbon nanotube film composite for active vibration control of cantilevered beam," *IEEE Sensors J.*, vol. 19, no. 7, pp. 2466–2473, Apr. 2019.

[12] H.-C. Wang, K.-C. Chuang, and C.-C. Ma, "Experimental study of active vibration control for suppressing impact or moving disturbance-induced vibrations with polyvinylidene fluoride and fiber Bragg grating sensors," *Sensors Actuators A: Phys.*, vol. 272, pp. 349–3461, 2018.
[13] T. Kebabsa, N. Ouelaa, and A. Djebala, "Experimental vibratory analysis of a fan motor in industrial environment," *Int. J. Adv. Manuf. Technol.*, vol. 98, pp. 2439–2447, 2018.
[14] I. Abu-Mahfouz and A. Banerjee, "Crack detection and identification using vibration signals and fuzzy clustering," *Procedia Comput. Sci.*, vol. 114, pp. 266–274, 2017.
[15] D. Dongmei, H. Qing, and T. Bing, "ARM-based handheld analyzer for vibration," in *Proc. 2nd Int. Conf. Inf. Comput. Sci.*, 2009, pp. 381–384.
[16] V. Kumar, A. Abbasalipour, A. Ramezany, and S. Pourkamali, "A low-power CMOS-MEMS vibration spectrum analyzer," in *Proc. IEEE Int. Freq. Control Symp.*, 2018, pp. 1–4.
[17] A. Naha, K. R. Thammayyabbabu, A. K. Samanta, A. Routray, and A. K. Deb, "Mobile application to detect induction motor faults," *IEEE Embedded Syst. Lett.*, vol. 9, no. 4, pp. 117–120, Dec. 2017.
[18] S. Hodgson, M. Tavakoli, M. T. Pham, and A. Leleve, "Nonlinear discontinuous dynamics averaging and PWM-based sliding control of solenoid-valve pneumatic actuators," *IEEE/ASME Trans. Mechatronics*, vol. 20, no. 2, pp. 876–888, Apr. 2015.
[19] L. Wang and J. Ma, "A kurtosis and skewness based criterion for model selection on Gaussian mixture," in *Proc. 2nd Int. Conf. Biomed. Eng. Inform.*, 2009, pp. 1–5.
[20] J. P. LeBlanc and P. L. D. Leon, "Speech separation by kurtosis maximization," in *Proc. IEEE Int. Conf. Acoust. Speech, Signal Process.*, 1998, pp. 1029–1032.
[21] M. M. Hittawe, S. M. Muddamsetty, D. Sidibé, and F. Mériaudeau, "Multiple features extraction for timber defects detection and classification using SVM," in *Proc. IEEE Int. Conf. Image Process.*, 2015, pp. 427–431.
[22] Y. He, K. Song, Q. Meng, and Y. Yan, "An end-to-end steel surface defect detection approach via fusing multiple hierarchical features," *IEEE Trans. Instrum. Meas.*, vol. 69, pp. 1493–1504, Apr. 2020.
[23] A. H. Jahromi and M. Taheri, "A non-parametric mixture of Gaussian naive bayes classifiers based on local independent features," in *Proc. Artif. Intell. Signal Process. Conf.*, 2017, pp. 209–212.

CHAO-CHUNG PENG was born in Kaohsiung, Taiwan, in 1980. He received the B.S. and Ph.D. degrees from the Department of Aeronautics and Astronautics, National Cheng Kung University (NCKU), Tainan, Taiwan, in 2003 and 2009, respectively. From 2008 to 2009, he was a Research Assistant with the Department of Engineering, Leicester University, Leicester, U.K. From 2010 to 2012, he was a Postdoctoral Fellow with the Department of Mechanical Engineering, NCKU. In 2012, he was a Senior Engineer with Embedded System Development Section, Measurement and Automation Department, ADLINK Technology, Taipei, Taiwan. From 2014 to 2016, he was with Automation and Instrumentation System Development Section, Iron & Steel Research and Development Department, China Steel Corporation, Kaohsiung, Taiwan. Since 2016, he has been an Assistant Professor with the Department of Aeronautics and Astronautics, NCKU. In 2020, he was promoted as an Associated Professor. His research interests include high-performance motion control and applications, unmanned vehicle design, advanced flight control system development, autonomous robotics, intelligence simultaneous localization and mapping (SLAM) technology, system modeling, and diagnosis. He was awarded a membership in the Phi Tau Phi Scholastic Honor Society, in 2009 and the Excellent Young Engineering Professor Award by Chinese Society of Mechanical Engineers (CSME), in 2019.